



Since January 2020 Elsevier has created a COVID-19 resource centre with free information in English and Mandarin on the novel coronavirus COVID-19. The COVID-19 resource centre is hosted on Elsevier Connect, the company's public news and information website.

Elsevier hereby grants permission to make all its COVID-19-related research that is available on the COVID-19 resource centre - including this research content - immediately available in PubMed Central and other publicly funded repositories, such as the WHO COVID database with rights for unrestricted research re-use and analyses in any form or by any means with acknowledgement of the original source. These permissions are granted for free by Elsevier for as long as the COVID-19 resource centre remains active.

available at www.sciencedirect.comjournal homepage: www.elsevier.com/locate/biochempharm

Thiopurine analogues inhibit papain-like protease of severe acute respiratory syndrome coronavirus

Chi-Yuan Chou^a, Chia-Hui Chien^b, Yu-San Han^{b,1}, Mojca Trstenjak Prebanda^c,
Hsing-Pang Hsieh^b, Boris Turk^c, Gu-Gang Chang^a, Xin Chen^{b,*}

^aDepartment of Life Sciences and Institute of Genome Sciences, National Yang-Ming University, Taipei 112, Taiwan, ROC

^bDivision of Biotechnology and Pharmaceutical Research, National Health Research Institutes, No. 35 Keyan Rd., Zhunan town, Miaoli County 350, Taiwan, ROC

^cDepartment of Biochemistry, Molecular and Structural Biology, J. Stefan Institute, Jamova 39, SI-1000 Ljubljana, Slovenia

ARTICLE INFO

Article history:

Received 6 November 2007

Accepted 11 January 2008

Keywords:

Severe acute respiratory syndrome coronavirus

Papain-like proteinase 2

Inhibitor

6-Mercaptopurine

6-Thioguanine

Cysteine protease

ABSTRACT

The papain-like protease of severe acute respiratory syndrome coronavirus (PLpro) (EC 3.4.22.46) is essential for the viral life cycle and therefore represents an important antiviral target. We have identified 6MP and 6TG as reversible and slow-binding inhibitors of SARS-CoV PLpro, which is the first report about small molecule reversible inhibitors of PLpro. The inhibition mechanism was investigated by kinetic measurements and computer docking. Both compounds are competitive, selective, and reversible inhibitors of the PLpro with K_{is} values ~ 10 to $20 \mu\text{M}$. A structure–function relationship study has identified the thiocarbonyl moiety of 6MP or 6TG as the active pharmacophore essential for these inhibitions, which has not been reported before. The inhibition is selective because these compounds do not exert significant inhibitory effects against other cysteine proteases, including SARS-CoV 3CLpro and several cathepsins. Thus, our results present the first potential chemical leads against SARS-CoV PLpro, which might be used as lead compounds for further optimization to enhance their potency against SARS-CoV. Both 6MP and 6TG are still used extensively in clinics, especially for children with acute lymphoblastic or myeloblastic leukemia. In light of the possible inhibition against subset of cysteine proteases, our study has emphasized the importance to study in depth these drug actions in vivo.

© 2008 Elsevier Inc. All rights reserved.

1. Introduction

Severe acute respiratory syndrome (SARS) is a life-threatening atypical pneumonia caused by the SARS coronavirus (SARS-CoV) [1]. During the outbreak in 2003, this virus infected more than 8000 people, and the fatality rate in humans was as high as 15% (World Health Organization). Its

easy transmissibility between humans makes the reemergence of SARS-CoV a distinct possibility, which entails an urgent need to prepare antiviral drugs against SARS-CoV. To date, there is no effective anti-SARS drug available with proven efficacy in vivo [2], although vaccines and monoclonal antibodies against SARS-CoV are being developed [3,4].

* Corresponding author. Tel.: +886 37 246166x35718; fax: +886 37 586456.

E-mail address: xchen@nhri.org.tw (X. Chen).

¹ Present address: Institute of Fisheries Science, College of Life Science, National Taiwan University, Taipei, Taiwan 106, ROC.

Abbreviations: SARS, severe acute respiratory syndrome; CoV, coronavirus; PLpro, papain-like proteinase 2; 3CLpro, 3-chymotrypsin-like protease; DUB, deubiquitination enzyme; AMC, 7-amino-4-methylcoumarin; FRET, fluorescence resonance energy transfer; 6MP, 6-mercaptopurine; 6TG, 6-thioguanine.

0006-2952/\$ – see front matter © 2008 Elsevier Inc. All rights reserved.

doi:10.1016/j.bcp.2008.01.005

SARS-CoV is a plus-strand RNA virus encoding four structural proteins, 16 nonstructural proteins, and 8 accessory proteins [5]. The 16 nonstructural proteins are the cleavage products of the 2 large polypeptides pp1a and pp1ab, generated by the virally encoded proteases 3-chymotrypsin-like protease (3CLpro) and papain-like protease (PLpro) (EC 3.4.22.46). SARS-CoV also encodes a helicase with multiple enzymatic activities in vitro, including RNA/DNA helicase, nuclease, and RNA 5'-triphosphatase activities, and an RNA-dependent RNA polymerase [6]. Extensive and in-depth investigation of SARS-CoV has led to the identification of its cellular receptor, carboxypeptidase angiotensin-converting enzyme 2 [7]; the determination of the structures of many viral structural and nonstructural proteins [5]; and an understanding of the functions of many of these viral proteins in vivo [6,8].

An intensive hunt for effective anti-SARS drugs has been undertaken, including the screening of existing antiviral or other marketed drugs for possible anti-SARS effects [9]. Inhibitors have been both designed and discovered by targeting different components of the virus, including the interaction between the viral S protein and the host receptor, which mediates fusion and viral entry [10], cathepsin L (to decrease membrane fusion) [11], 3CLpro [9], RNA-dependent RNA polymerase [12,13], and helicase [14,15]. So far, these compounds have been predominantly tested for their in vitro efficacy and no human clinical trials have ever been initiated. Recently, an animal model mimic the mortality and human disease syndrome as induced by a mouse-adapted SARS-CoV has been set up [16], which will provide the opportunity to test the effectiveness of the inhibitors for in vivo efficacy. Proteases remain one of the most prominent and effective drug targets in antiviral therapies, including those directed against human immunodeficiency virus, hepatitis C virus, and other viral infections [17,18]. Because proteolytic processing is essential for the generation of a functional replication complex, 3CLpro and PLpro are potentially effective targets for anti-SARS drugs. Most efforts reported until now have focused on the development of 3CLpro inhibitors [9]. However, except our previous observation that the zinc ion inhibits PLpro of SARS-CoV [19], no inhibitor of this protease has yet been reported.

PLpro of SARS-CoV is a papain-like cysteine protease with deubiquitinating activity. It is located on polypeptide 1a and self-cleaves at three sites on the polypeptide. Its catalytic triad (Cys1651–His1812–Asp1826) has a broad range of pH optima, characteristic of papain-like cysteine proteases [19,20]. Moreover, PLpro has deubiquitinating activity in vitro, and is capable of hydrolyzing diubiquitin, polyubiquitin, and synthetic ubiquitin peptide substrates [20,21]. Recently, its crystal structure has been solved, and it shows great similarity to those of two other mammalian deubiquitinating enzymes (DUBs), USP14 and herpesvirus-associated ubiquitin-specific protease (HAUSP) [22–24]. Despite low sequence identity (around 10%), these three proteins share similar tripartite architectures, comprising finger, palm, and thumb domains. There is also a ubiquitin-like domain at the amino terminus of PLpro, which might be responsible for its association with 26S proteasomes, as has been observed for USP14 and a yeast DUB called ubp6 [25]. PLpro also has de-ISGylation activity [21]. ISG15 is a ubiquitin-like protein involved in the posttranslational modification of proteins. The biological functions of the

deubiquitination and de-ISGylation activities of PLpro and its in vivo substrates are unknown at present.

Previously, we developed a fluorescence resonance energy transfer (FRET) assay to screen the inhibitors of PLpro in a high-throughput format [19]. Here, we report the discovery that 6-mercaptapurine (6MP) and 6-thioguanine (6TG) inhibit SARS-CoV PLpro. 6MP and 6TG are purine analogues effective in the treatment of patients with acute lymphoblastic or myeloblastic leukemia [26,27]. Their structure–activity relationship and inhibition mechanisms were investigated. To our knowledge, these are the first chemical compounds reported to be reversible inhibitors of PLpro. The implications of using 6MP and 6TG in antiviral therapies are discussed.

2. Materials and methods

2.1. Materials

Ni-NTA agarose was from Qiagen, Inc., Valencia, CA, USA. The compound library used was the Genesis Plus Collection purchased from MicroSource Discovery Systems, Inc., Gaylordville, CT, USA. This library contains many compounds already approved by the United States Food and Drug Administration (FDA). 6-Thioguanine (6TG), hypoxanthine, 6-methylmercaptapurine, and N-ethylmaleimide (NEM) were from Sigma-Aldrich Corporation, Inc., Louis, ST, USA. 6-Mercaptapurine (6MP) was from Fluka, Inc., Buchs, SG, Switzerland, and 2-amino-6-methylmercaptapurine was from Acros Organics, Thermo Fisher Scientific Inc., Waltham, MA, USA. Papain-like cysteine protease cathepsins B, L, K and S were prepared as described previously [28–30] whereas papain was from Sigma-Aldrich Corporation, Inc., and further purified to homogeneity [31]. All calpains tested in this study were active titrated with E-64 from Sigma-Aldrich Corporation, Inc. [32].

2.2. Purification of SARS-CoV PLpro and 3CLpro

The PLpro expression plasmid was constructed by amplifying the PLpro cDNA by PCR with the primers 5'-AAAGGATCCGCT-GAACTCTCTAAATG-3' and 5'-AAACTCGAGCGACACAGGCTT-GATG-3', using the previously constructed plasmid pBacPAK8-PLpro as a template [19]. The cDNA fragment was released with BamHI and XhoI digestion before it was ligated into the pET-22b vector with a 6× His tag at the C terminus (Novagen). PLpro was expressed in *Escherichia coli* BL21 (DE3). The cells were induced with 1 mM isopropyl-1-thio-β-D-galactose (IPTG) and cultured at 16 °C overnight, before they were collected by centrifugation at 6000 × g at 4 °C for 10 min. The cell pellets were sonicated in buffer containing 4 mM imidazole, 300 mM sodium chloride, and 20 mM Tris-HCl (pH 7.9), before the suspension was cleared by centrifugation at 10,000 × g for 25 min at 4 °C. The supernatant was incubated with a 50% Ni-NTA slurry (Qiagen) at 4 °C for 60 min and loaded into a column. The column was washed with buffer containing 30 mM imidazole, 300 mM sodium chloride, and 20 mM Tris-HCl (pH 7.9). PLpro protein was eluted with buffer containing 400 mM imidazole, 300 mM sodium chloride, and 20 mM Tris-HCl (pH 7.9). The protein was stored in 50 mM phosphate buffer (pH 7.4), after buffer exchange with an Amicon Ultra-4

centrifugal filter device (Millipore). Typical yield of the protein was 2 mg per liter of cell culture. Purification and measurement of the enzymatic activity of 3CLpro of SARS-CoV were performed as described previously [33].

2.3. Inhibitor-screening platform and deubiquitination assay

Inhibitor screening was carried out as described previously [19]. For the deubiquitination assay, PLpro (40 nM) was incubated with the chemical compounds for 10 min before the substrate, ubiquitin-AMC (1 μ M), was added in 50 mM phosphate buffer (pH 6.8). The enzymatic activities were determined by monitoring the enhanced fluorescence emission upon substrate cleavage at excitation and emission wavelengths of 380 and 436 nm, respectively, in a PerkinElmer LS 50B luminescence spectrometer (USA).

2.4. Steady-state kinetic analysis

Because it is slightly more soluble in the assay buffer, we used DabcyI-FRLKGGAPIKGV-Edans instead of Abz-FRLKGGAPIKGV-Edans [19] as the substrate to measure the enzymatic activity of PLpro throughout the course of the study as described [19]. Specifically, the enhanced fluorescence emission upon substrate cleavage was monitored at excitation and emission wavelengths of 329 and 520 nm, respectively, in a PerkinElmer LS 50B luminescence spectrometer. Fluorescence intensity was converted to the amount of hydrolyzed substrate using a standard curve drawn from the fluorescence measurements of well-defined concentrations of DabcyI-FRLKGG and APIKGV-Edans peptides in a 1:1 ratio. This will also correct for the inner filter effect of the substrate. For the kinetic analysis, the reaction mixture contained 0.5–25 μ M peptide substrate in 50 mM phosphate buffer (pH 6.2, 6.8, or 8.0) in a total volume of 1 mL. After the addition of the enzyme to the reaction mixture, the increase in fluorescence at 520 nm (excited at 329 nm) was continuously monitored at 30 °C with a PerkinElmer LS 50B luminescence spectrometer. The increase in fluorescence was linear for at least 10 min, and thus the slope of the line represented the initial velocity (v). The steady-state kinetic parameters of the enzyme were determined by fitting the Michaelis–Menten equation (Eq. (1)) to the initial velocity data

$$v = \frac{V_{\max}[S]}{K_m + [S]} \quad (1)$$

in which V_{\max} is the maximum reaction rate, $[S]$ denotes the substrate concentration, and K_m is the Michaelis–Menten constant for the interaction between the peptide substrate and the enzyme.

For the inhibition studies, 5–50 μ M peptide substrate and 0–100 μ M 6MP or 6TG were mixed with PLpro (0.1 μ M) at 30 °C, and the fluorescence intensity was monitored. Specifically, the enhanced fluorescence emission upon substrate cleavage was monitored at excitation and emission wavelengths of 329 and 520 nm, respectively, in a PerkinElmer LS 50B luminescence spectrometer. Fluorescence intensity was converted to the amount of hydrolyzed substrate using a standard curve drawn from the fluorescence measurements of well-defined con-

centrations of DabcyI-FRLKGG and APIKGV-Edans peptides in a 1:1 ratio, and the enzymatic activity was assayed. The inhibition data were best fitted to a competitive inhibition pattern according to Eq. (2)

$$v = \frac{V_{\max}[S]}{(1 + [I]/K_{is})K_m + [S]} \quad (2)$$

in which $[I]$ is the inhibitor concentration and K_{is} is the slope inhibition constant for the enzyme–inhibitor complex.

2.5. Inactivation mechanism

For the inactivation studies using 6MP, PLpro enzyme (0.1 μ M) in 50 mM phosphate buffer (pH 6.2) was incubated with different concentrations of 6MP (2–200 μ M) at 30 °C for 2 h. Aliquots were withdrawn at different time points and added to an assay mixture containing 50 μ M peptide substrate to determine the remaining enzyme activity. Substrate hydrolysis in the presence of inhibitor was linear for the first 10 min, and a good fit of the pseudo-first-order rate equation (Eq. (3)) to experimental data was obtained

$$-\ln(E_t/E_0) = k_{\text{inact}}t \quad (3)$$

in which E_0 is the enzyme activity at time zero and E_t is the enzyme activity at time t . The slope of this semi-log plot represents the observed inactivation rate constant (k_{inact}). To study its inactivation by 6TG, PLpro enzyme (0.1 μ M in 50 mM phosphate buffer (pH 6.2) was incubated with different concentrations of 6TG (5–100 μ M) at 30 °C in the presence of the peptide substrate, and the enzymatic activity was traced for 10 min. All the progress curves recorded showed an exponential approach to a final linear rate and were analyzed by the least-squares fitting of the following integrated rate equation (Eq. (4); Ref. [34]) to the experimental data:

$$[P] = v_s t + \frac{v_i + v_s}{k_{\text{inact}}} [1 - \exp(-k_{\text{inact}}t)] + d \quad (4)$$

in which v_i is the initial velocity, v_s is the steady-state velocity, and d is the displacement on the y-axis.

The replot of k_{inact} versus 6MP or 6TG concentration was not linear and was therefore fitted to a saturation curve, according to Eq. (5) [34,35]

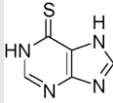
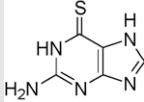
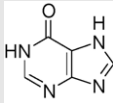
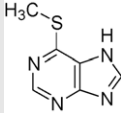
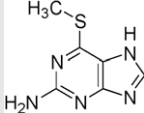
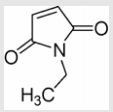
$$k_{\text{inact}} = \frac{k_{\max}[I]}{K_{\text{inact}} + [I]} \quad (5)$$

in which K_{inact} is the dissociation constant of the enzyme–6MP or enzyme–6TG complex and k_{\max} is the maximum inactivation rate constant.

2.6. Computer modeling of PLpro in a complex with 6MP or 6TG

The crystal structures of SARS-CoV PLpro (pdb code: 2FE8) [24] and 3CLpro (pdb code: 1UK2) were used as the templates. Docking was performed with DS Modeling 1.7 software (Accelrys). Before docking, the size space of 110 Å³ (891 grid

Table 1 – Structure–activity relationships of compounds against SARS-CoV PLpro

Number	Name	Structure	IC ₅₀ (μM)
1	6-Mercaptopurine (6MP)		21.6 ± 1.8
2	6-Thioguanine (6TG)		5.0 ± 1.7
3	Hypoxanthine		ND ^a
4	6-Methyl-mercaptopurine		ND ^a
5	2-Amino-6-methyl-mercaptopurine		ND ^a
6	NEM		4.4 ± 1.0

^a ND: IC₅₀ values were not determined due to the lack of inhibition.

points) near the active site was chosen. The structures of 6MP and 6TG were created and separately specified as input ligands. During the docking experiment, the chemical flexibility of 6MP or 6TG was allowed, and the interaction energy was adopted as the force field and charging method. The grid extension from the site was 3.0 Å, and the nonbonded cutoff distance was 10.0 Å. The softened potential energy and distance-dependent dielectric were used (the dielectric constant was 1.0). The docking results were calibrated by Monte Carlo trials, in which maximal torsion of 25 and possible poses of 10 were compared.

3. Results

3.1. Identification of inhibitors of SARS-CoV PLpro

We expressed and purified PLpro from *E. coli* as described in Section 2. The purified protease ran at around 52 kDa on sodium dodecyl sulfate–polyacrylamide gel electrophoresis, with over 90% purity (data not shown). MASS analysis was also carried out to determine the homogeneity of the enzyme preparation. Single peak around the molecular mass of 52,346 was observed, close to the predicted 52,645 Da (data not shown). When assayed with the peptide substrate under conditions similar to those reported previously [19], the PLpro from this preparation exhibited very similar kinetic properties to the PLpro isolated from insect cells with the specific activity

of 130 μMol min⁻¹ mg⁻¹ using the substrate Dabcyl–FRLKGGAPIKGV–Edans, as compared to that of 404 μMol min⁻¹ mg⁻¹ from insect cells using the substrate Abz–FRLKGGAPIKGV–Edans [19], suggesting that the expression system had no major influence on the properties.

To identify potent inhibitors of SARS-CoV PLpro, we screened a library containing 960 compounds using a screening platform that we had established previously [19]. Interestingly, we found that, apart from the zinc ion [19], thiocarbonyl-containing 6MP (compound 1) and 6TG (compound 2) were effective inhibitors of SARS-CoV PLpro, with IC₅₀ values of 21.6 and 5 μM, respectively (Table 1). NEM (compound 6), a commonly used cysteine protease inhibitor that acts by covalently modifying the active-site Cys through Michael addition, was also found to be an effective inhibitor of PLpro with an IC₅₀ value of 4.4 μM, however, it was not further investigated. Because PLpro is a deubiquitination enzyme with a structure highly homologous to those of other DUBs [20,21,24], we next tested whether 6MP and 6TG also inhibited the deubiquitinating activity of PLpro. Using ubiquitin–AMC as the substrate, we found that 6MP, 6TG, and Zn²⁺ effectively inhibited the deubiquitinating activity of PLpro (Fig. 1). To determine whether this inhibition is reversible, we first incubated the enzyme with both 6MP and 6TG until no activity of the enzyme could be detected. Next, the enzyme was purified with gel filtration, followed by new activity measurement. The enzymatic activity was restored, suggesting that the enzyme–inhibitor complex dissociated on the column

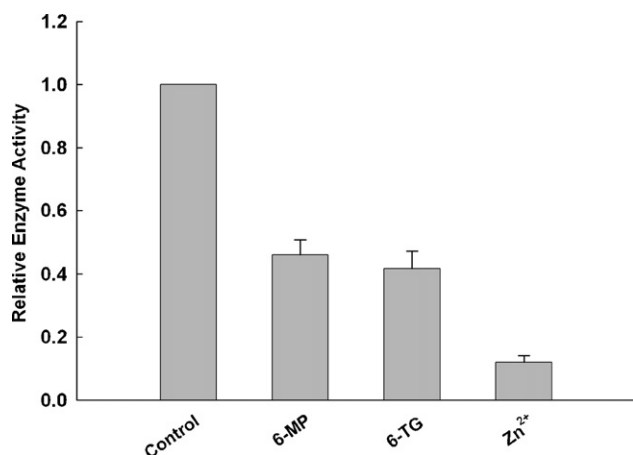


Fig. 1 – Inhibition of PLpro deubiquitination activity by thiopurines and Zn²⁺. The percentages of PLpro activity remaining after treatment with 6MP, 6TG, or Zn²⁺ were measured. The fluorogenic substrate ubiquitin-AMC (1 μ M) was used as the substrate.

and/or by dilution in the assay buffer, which is indicative of reversible inhibition.

To identify the active pharmacophore in the inhibition, a structure–function relationship study was carried out. A substructure search based on the structures of 6MP and 6TG was carried out using the software ISIS (<http://www.isis.rl.ac.uk/dataanalysis/>) against the MDL Available Chemical Directory (MDL ACD). Since the major difference between adenosine and 6MP/6TG lies in the thiocarbonyl group, we searched for the different substituted group at this site in the database. Compounds 3, 4 and 5 were discovered and available to purchase commercially (Section 2). Replacement of the thiocarbonyl of 6MP or 6TG with either hydroxyl (compound 3) or a methylthio group (compounds 4 and 5) resulted in compounds devoid of inhibitory activity (Table 1), suggesting that the thiocarbonyl group of 6MP or 6TG is the active pharmacophore for the inhibition. To gain further insight into the inhibition mechanism, a docking experiment was performed. PLpro exists as a monomer in solution [19]. In the crystallization form, there are three monomers existing in the asymmetric unit [24]. The active sites for all three units were the same (data not shown). So we chose subunit one for the modeling study. Both 6MP and 6TG fit well into the active-site cavity of PLpro. The sulfur atom of 6MP or 6TG was juxtaposed closely with the γ -S of Cys1651 at a distance of 3.4 Å, suggesting possible formation of a hydrogen bond (Fig. 2). This is consistent with the active chemical properties of the thiocarbonyl group. The best docking scores for 6MP and 6TG binding to PLpro were 23.9 and 24.4, respectively. Moreover, the binding energies of 6MP and 6TG to PLpro were 8.2 and 14.7 kcal/mol, respectively.

3.2. Inhibition mechanism

To understand the kinetic mechanism of the interaction of 6MP or 6TG with the enzyme, the enzymatic activity was measured with a series of substrate concentrations and

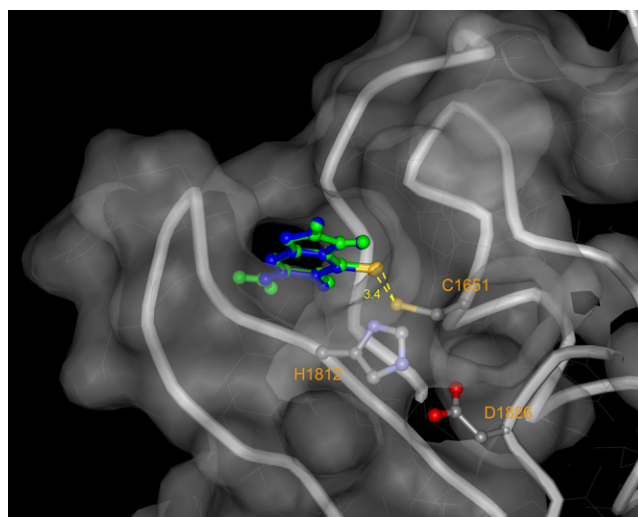


Fig. 2 – Docking and inhibition mechanism of 6MP and 6TG with PLpro. 6MP (colored blue) and 6TG (green) could be targeted to the active site of PLpro. The distances between the sulfur atom of the active-site Cys1651 and the sulfur atoms of 6MP or 6TG were all 3.4 Å.

various inhibitor concentrations. The inhibition data were globally fitted to all possible kinetic models (competitive, noncompetitive, uncompetitive and mixed competitive). As shown in Fig. 3, a simple competitive inhibition pattern best described the data for the following two reasons: (i) the double reciprocal plot with all lines intercepted the y-axis for both 6MP (Fig. 3A) and 6TG (Fig. 3B) and (ii), the slope versus inhibitor concentration replot was linear (Fig. 3, both insets). Therefore, consistent with the docking result (Fig. 2), both 6MP and 6TG may compete with the peptide substrate for the active site via a competitive mechanism. The best fit of Eq. (2) to experimental data yielded K_{is} values of 19 and 13 μ M for 6MP and 6TG, respectively (Table 2). As summarized in Table 2, in the pH range from 6.2 to 8.0, which was shown previously to be optimal for the enzymatic activity of PLpro [19], the K_m values for substrate hydrolysis in the absence of inhibitors ranged from 17 to 25 μ M, whereas the k_{cat} values ranged from 0.06 to 0.13 s^{-1} . The Michaelis constant (K_m) for the substrate and inhibition constant for 6MP and 6TG (K_{is} or K_{inact}) were similar.

To understand the kinetic mechanism of this inhibition, a time-dependent change in enzyme activity as a function of the inhibitor concentration was determined by preincubating the PLpro enzyme with different concentrations of the inhibitors at 30 °C prior to measuring the enzyme activity. For 6MP, the semi-log plots of E_t/E_0 versus time were linear in the initial stage (Fig. 4A), and the pseudo-first-order rate constant (k_{inact}) at different inhibitor concentrations followed saturation kinetics (Fig. 4C). For 6TG, the emission curve was curved downwards, indicating a slow-binding mechanism (Fig. 4B). By fitting the data to Eq. (4) for 6TG (Fig. 4B) (Section 2), different k_{inact} values at various concentration of 6TG were determined (Fig. 4D). When we further fitted the saturated curvature to Eq. (5), we determined that the K_{inact} values for 6MP and 6TG

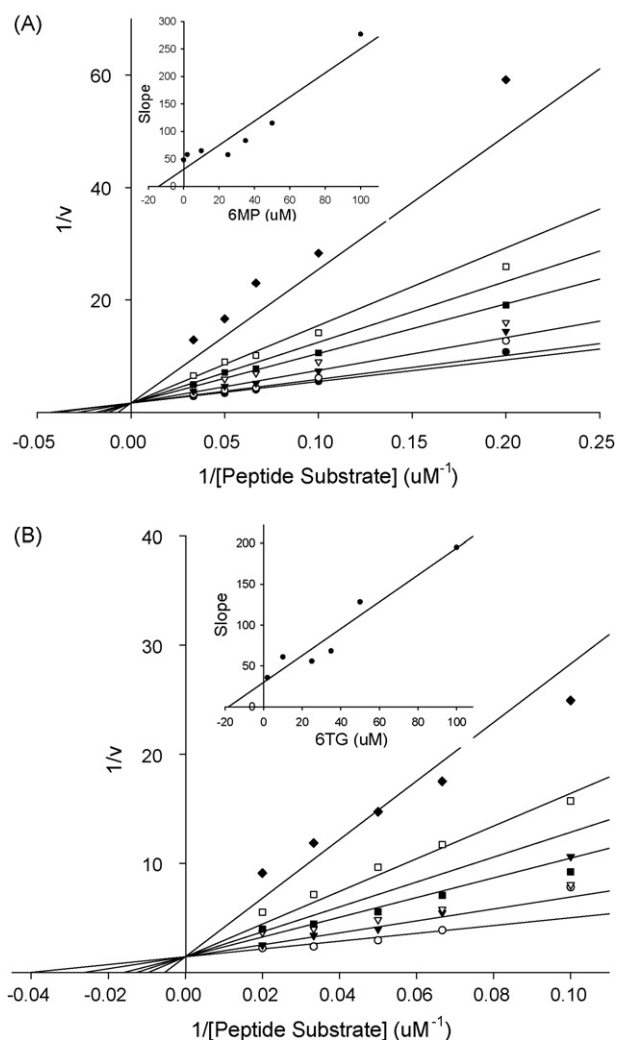


Fig. 3 – Competitive inhibition of PLpro by 6MP or 6TG. (A) 6MP; (B) 6TG. The inset figures represent [6MP] or [6TG] vs. slope replots. The enzymatic activity of PLpro was measured in the presence of different peptide substrate concentrations (5–50 μM) and various inhibitor concentrations: 0 (closed circles), 2 (open circles), 10 (closed triangles), 25 (open triangles), 35 (closed squares), 50 (open squares), 100 (closed diamonds) μM . The solid lines are the best fit by the competitive inhibition equation (Eq. (2)). $R_{\text{sqR}} = 0.920$ and 0.929 , respectively. The same experiments were repeated at least three times. The kinetic parameters such as K_m , k_{cat} and K_{is} from the best fit were shown in Table 2.

were 48 and 32 μM , respectively, and the k_{max} of inactivation were 0.12 and 0.92 ms^{-1} , respectively (Table 2). 6TG is a slightly more potent inhibitor than 6MP, as indicated by a slightly lower K_{inact} and a eight-fold higher k_{max} . In summary, both 6MP and 6TG are slow-binding inhibitors of SARS-CoV PLpro, although both 6MP and 6TG have binding affinities for PLpro similar to that of the peptide substrate (Table 2). Based on the above kinetic and modeling results, we propose the following kinetic mechanism (Fig. 5). 6MP or 6TG might form a hydrogen bond with the enzyme's active site Cys1651 through the thio moiety of the thiocarbonyl group. The hydrogen bonding with Cys1651 blocks the essential sulfhydryl group, preventing its acylation and inhibiting the enzyme's activity.

3.3. Activity of the inhibitors against other cysteine proteases

Next, we investigated whether 6MP and 6TG inhibit other cysteine proteases. Initially, the other SARS-CoV protease 3CLpro, which is also a cysteine protease, was tested for possible inhibition by 6MP and 6TG. A comparison with PLpro was therefore made at 200 μM inhibitor concentration and a 2 h incubation time. Whereas both inhibitors at this concentration almost completely abolished the activity of PLpro (<5% residual activity), they were found to be much less effective inhibitors of 3CLpro (49% residual activity for 6MP and 25% for 6TG, respectively). In the next step, we also used molecular modeling to dock the inhibitors to 3CLpro. The best docking scores for 6MP and 6TG to 3CLpro were 17.8 and 18.4, respectively, which are lower than those for 6MP and 6TG (23.9 and 24.4, respectively). Moreover, the binding energies of 6MP and 6TG to 3CLpro were -14.7 and -16.2 kcal/mol, respectively, which are lower than those to PLpro (8.2 and 14.7 kcal/mol, respectively). Finally, the sulfur atoms of 6MP and 6TG occur at distances of 5.4 and 8.5 \AA , respectively, from the $\gamma\text{-S}$ of Cys145 of 3CLpro, too far away to maintain a functional hydrogen bond. Therefore, the lower binding energies, lower docking scores, and greater distances of the drugs from 3CLpro are consistent with the biochemical data that these two drugs are not effective inhibitors of 3CLpro. Moreover, 6MP and 6TG were not effective inhibitors of other cysteine proteases, including cathepsins B, K, L, and S, and papain, even at a concentration of 1 mM (data not shown). Therefore, it seems that 6MP and 6TG are reasonably selective inhibitors of PLpro and do not inhibit other cysteine proteases.

Table 2 – Kinetic parameters of 6MP and 6TG inhibition of PLpro

PLpro in	K_m (μM) ^a	k_{cat} (s^{-1}) ^a	k_{cat}/K_m ($10^{-3} \text{ s}^{-1} \mu\text{M}^{-1}$)	K_{is} (μM) ^a	K_{inact} (μM) ^b	k_{max} (10^{-4} s^{-1}) ^b
pH 6.2	22.7 \pm 3.0	0.13 \pm 0.01	5.7 \pm 0.9			
pH 6.8	25.2 \pm 5.1	0.11 \pm 0.02	4.4 \pm 1.2			
pH 8.0	17.4 \pm 6.9	0.06 \pm 0.01	3.4 \pm 1.5			
6MP	23.2 \pm 3.1	0.13 \pm 0.01	5.6 \pm 0.9	19.2 \pm 1.6	48.3 \pm 7.0	1.2 \pm 0.1
6TG	21.5 \pm 6.1	0.14 \pm 0.02	6.5 \pm 2.0	13.0 \pm 2.8	32.4 \pm 7.1	9.2 \pm 0.9

^a The steady-state kinetic parameters of PLpro at different pH environments were determined by the Michaelis-Menten equation (Eq. (1)). In the presence of 6MP or 6TG, those of parameters and K_{is} were determined by the competitive inhibition model (Eq. (2)) (Fig. 3).

^b The K_{inact} and k_{max} were from the best fit to the saturation equation (Eq. (5)) (Fig. 4).

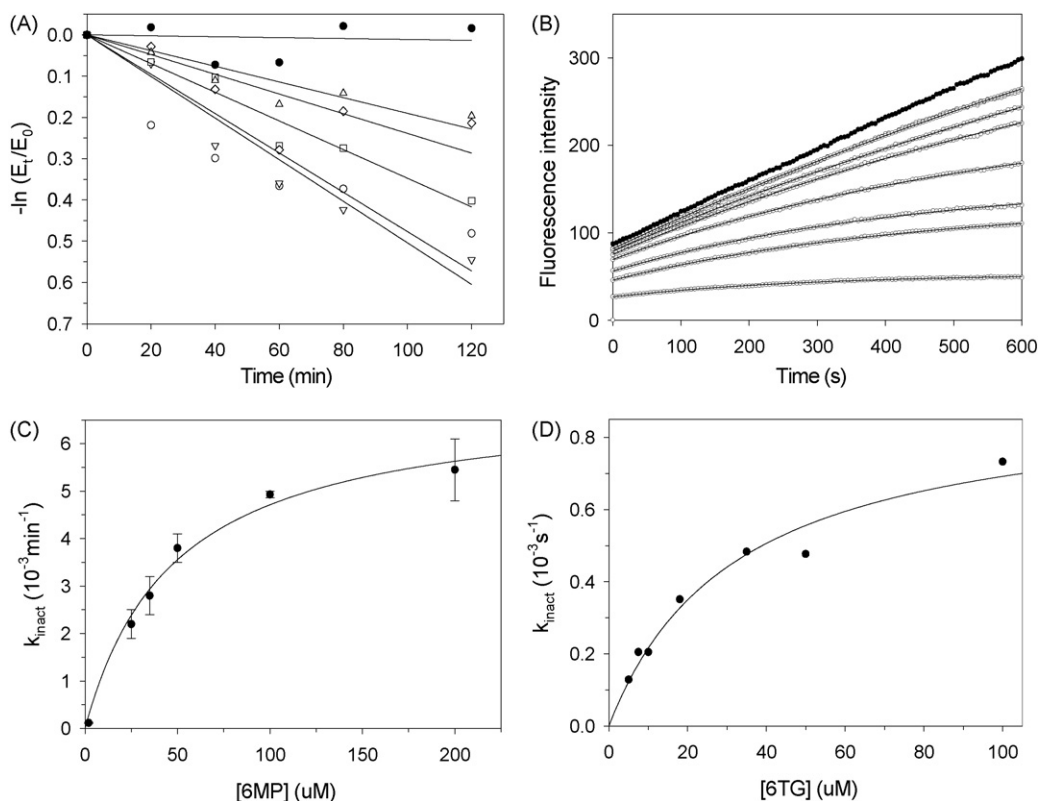


Fig. 4 – Time-dependent inactivation of PLpro by 6MP and 6TG. (A) Different concentrations of 6MP (2 μM , closed circles; 25 μM , triangles; 35 μM , diamonds; 50 μM , squares; 100 μM , invert triangles; and 200 μM , open circles) was incubated with PLpro for 2 h. E_t/E_0 indicates the residual enzymatic activity at time t . The solid lines show the best semi-log fits of the data at different 6MP concentrations by pseudo-first-order rate equation (Eq. (3)). (B) Different concentrations of 6TG (0 μM , closed circles; 5–100 μM , open circles) were incubated with PLpro for 10 min. The solid lines were the best-fit results according to the slow-binding equation (Eq. (4)). (C and D) The observed inactivation rate constants (k_{inact}) from panels A and B were replotted against 6MP or 6TG concentration. The solid line is the fit of the saturation equation (Eq. (5)) ($R_{\text{sq}} = 0.992$ and 0.975, respectively). The best-fit parameters (k_{inact} and k_{max}) are shown in Table 2. The same experiments were repeated at least three times.

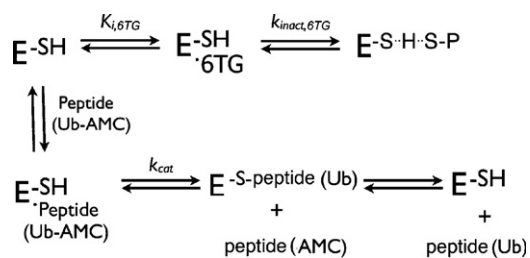


Fig. 5 – Kinetic mechanism of inhibitors. The upper part denotes enzyme inhibition and inactivation by 6TG (or 6MP). The lower part shows the putative hydrolysis of peptide substrate pathway. The original peptide substrate Dabcyl-FRLKGGAPIKGV-Edans (or ubiquitin-AMC) was cleaved at the Gly-Ala (or Gly-AMC) peptide bond. The N-terminal half (or AMC) was released as the first product while the C-terminal half (or ubiquitin) acylated the active site Cys1651, which was then deacylated and completed the catalytic cycle.

4. Discussion

6MP and 6TG are used clinically to treat leukemia. 6MP is a purine analogue, effective as an anticancer therapy because it is converted to 6TG nucleotides by hypoxanthine phosphoribosyl transferase in vivo. 6TG is then incorporated into DNA, preventing further replication. To our knowledge, 6MP and 6TG are the first reversible chemical inhibitors documented to inhibit PLpro of SARS-CoV, whereas many inhibitors have been developed for the other protease of SARS-CoV, 3CLpro [9].

In this study, we have identified these two compounds as slow-binding inhibitors of SARS-CoV PLpro, likely compete for the same binding site as the substrate. At the current stage, we could not rule out the possibility that the inhibition is through binding to an allosteric site thereby changing the conformation of the active site. Nevertheless, the inhibition is competitive, reversible and selective against PLpro. Although the affinity of 6MP and 6TG against PLpro is in the μM range, they could be used as lead compounds for further optimization to enhance their potency against SARS-CoV. There are many

such examples reported in the past of successful antiviral treatments with old drugs [36]. In light of the availability of several animal models [4], especially the one infected by a mouse-adapted SARS-CoV, which reproduces many aspects of the human disease including morbidity, mortality and pulmonary pathology [16]. It would be interesting to test whether these two drugs are effective in blocking SARS-CoV replication in these animal models.

Importantly, our structure–activity study (Table 1) has identified the thiocarbonyl group of 6MP and 6TG as the moiety for the inhibition of PLpro, which was not known before for these two compounds. In light of the acute toxicities associated with these drugs and the active thiocarbonyl against subsets of cysteine proteases, the *in vivo* action of 6MP and 6TG might be more complex than we realize at this stage. It is well documented that 6MP causes some adverse drug reactions in a significant number of patients, which have been found to be caused by a genetic polymorphism of thiopurine S-methyltransferase (TPMT). The polymorphism produces a TPMT with much lower activity [37,38]. These patients are less able to metabolize 6MP to the inactive 6-methyl mercaptopurine, resulting in the accumulation of 6TG and subsequent life-threatening myelosuppression [37–39]. About 1 in 300 individuals carries a mutated TPMT and does not express fully functional TPMT [40]. For these patients, less than 10% of the normal dosage of 6MP can be tolerated [39]. It is likely that locally high dosage of 6MP/6TG might inhibit the subset of cysteine proteases, thereby contributing to the severe cytotoxic effects observed by these two drugs. Furthermore, 6MP can also be metabolically processed by hepatic cytochrome P450 to purine-6-sulfenic acid, which binds to proteins by forming disulfide bonds with the thio moieties of the proteins both *in vitro* and *in vivo* [41,42]. Whether purine-6-sulfenic acid forms the disulfide bonds with cellular cysteine proteases remains to be studied.

We speculate that DUBs are the *in vivo* targets of 6MP and 6TG, based on our study of the mechanism of inhibition of PLpro, the selectivity of 6MP and 6TG, and the structural similarity of PLpro to other DUBs. To date, there is no potent selective chemical compound available for the inhibition of cellular deubiquitination enzymes other than a ubiquitin aldehyde developed for laboratory studies of the function of DUBs by covalent attachment to the active-site Cys [43,44]. Hence, the biological consequences of inhibiting DUBs are not clear at the moment. Moreover, the functions of the deubiquitination and de-ISGylation activities of PLpro *in vivo* are also unknown, as are those of its *in vivo* cellular substrates. Adenovirus encodes a deubiquitinating enzyme [45], which is necessary for processing viral precursor proteins during virion maturation [46]. ISGylation and de-ISGylation are involved in the innate immune response to viral infection [47]. Therefore, whether 6MP and 6TG inactivate the cellular DUBs that contribute to adverse drug reactions or other biological consequences requires further investigation. Because both drugs are still used extensively in clinics, especially for children with acute lymphoblastic or myeloblastic leukemia [26,27], our study has emphasized the importance to study in depth these drug actions *in vivo*.

Acknowledgements

We are grateful to Dr. Chun-Gong Jou, Dr. Yaw-Kun Li, Dr. Ke-Shan Shia, Dr. Hong-Yong Fu and Dr. Tsu-An Hsu for their help during the study. We would also like to thank Dr. Raymond S.L. Chang for critical reading and comment of the manuscript. This study was supported by National Science Council, Taiwan, ROC (grant 95-2320-B-010-013 to G.G. Chang, 93-2751-B-400-002-Y and 95-3112-B-400-010 of NRPGM to X.C.), and by Slovene Research Agency (grant P1-0140 to B.T.). We also thank NHRI for its financial support.

REFERENCES

- [1] Peiris JS, Guan Y, Yuen KY. Severe acute respiratory syndrome. *Nat Med* 2004;10:S88–97.
- [2] Stockman LJ, Bellamy R, Garner P. SARS: systematic review of treatment effects. *PLoS Med* 2006;3:e343.
- [3] Tsunetsugu-Yokota Y, Ohnishi K, Takemori T. Severe acute respiratory syndrome (SARS) coronavirus: application of monoclonal antibodies and development of an effective vaccine. *Rev Med Virol* 2006;16:117–31.
- [4] Roberts A, Lamirande EW, Vogel L, Jackson JP, Paddock CD, Guarner J, et al. Animal models and vaccines for SARS-CoV infection. *Virus Res* 2007.
- [5] Bartlam M, Yang H, Rao Z. Structural insights into SARS coronavirus proteins. *Curr Opin Struct Biol* 2005;15:664–72.
- [6] Tan YJ, Lim SG, Hong W. Characterization of viral proteins encoded by the SARS-coronavirus genome. *Antiviral Res* 2005;65:69–78.
- [7] Li W, Moore MJ, Vasilieva N, Sui J, Wong SK, Berne MA, et al. Angiotensin-converting enzyme 2 is a functional receptor for the SARS coronavirus. *Nature* 2003;426:450–4.
- [8] Tan YJ, Lim SG, Hong W. Understanding the accessory viral proteins unique to the severe acute respiratory syndrome (SARS) coronavirus. *Antiviral Res* 2006;72:78–88.
- [9] Wu YS, Lin WH, Hsu JT, Hsieh HP. Antiviral drug discovery against SARS-CoV. *Curr Med Chem* 2006;13:2003–20.
- [10] Yi L, Li Z, Yuan K, Qu X, Chen J, Wang G, et al. Small molecules blocking the entry of severe acute respiratory syndrome coronavirus into host cells. *J Virol* 2004;78:11334–9.
- [11] Simmons G, Gosalia DN, Rennekamp AJ, Reeves JD, Diamond SL, Bates P. Inhibitors of cathepsin L prevent severe acute respiratory syndrome coronavirus entry. *Proc Natl Acad Sci USA* 2005;102:11876–81.
- [12] He R, Adonov A, Traykova-Adonova M, Cao J, Cutts T, Grudesky E, et al. Potent and selective inhibition of SARS coronavirus replication by aurantricarboxylic acid. *Biochem Biophys Res Commun* 2004;320:1199–203.
- [13] Barnard DL, Hubbard VD, Burton J, Smee DF, Morrey JD, Otto MJ, et al. Inhibition of severe acute respiratory syndrome-associated coronavirus (SARSCoV) by calpain inhibitors and beta-D-N4-hydroxycytidine. *Antivir Chem Chemother* 2004;15:15–22.
- [14] Kao RY, Tsui WH, Lee TS, Tanner JA, Watt RM, Huang JD, et al. Identification of novel small-molecule inhibitors of severe acute respiratory syndrome-associated coronavirus by chemical genetics. *Chem Biol* 2004;11:1293–9.
- [15] Tanner JA, Zheng BJ, Zhou J, Watt RM, Jiang JQ, Wong KL, et al. The adamantane-derived bananins are potent inhibitors of the helicase activities and replication of SARS coronavirus. *Chem Biol* 2005;12:303–11.

- [16] Roberts A, Deming D, Paddock CD, Cheng A, Yount B, Vogel L, et al. A mouse-adapted SARS-coronavirus causes disease and mortality in BALB/c mice. *PLoS Pathog* 2007;3:e5.
- [17] De Clercq E. Strategies in the design of antiviral drugs. *Nat Rev Drug Discov* 2002;1:13–25.
- [18] Turk B. Targeting proteases: successes, failures and future prospects. *Nat Rev Drug Discov* 2006;5:785–99.
- [19] Han YS, Chang GG, Juo CG, Lee HJ, Yeh SH, Hsu JT, et al. Papain-like protease 2 (PLP2) from severe acute respiratory syndrome coronavirus (SARS-CoV): expression, purification, characterization, and inhibition. *Biochemistry* 2005;44:10349–5.
- [20] Barretto N, Jukneliene D, Ratia K, Chen Z, Mesecar AD, Baker SC. The papain-like protease of severe acute respiratory syndrome coronavirus has deubiquitinating activity. *J Virol* 2005;79:15189–98.
- [21] Lindner HA, Fotouhi-Ardakani N, Lytvyn V, Lachance P, Sulea T, Menard R. The papain-like protease from the severe acute respiratory syndrome coronavirus is a deubiquitinating enzyme. *J Virol* 2005;79:15199–208.
- [22] Hu M, Li P, Li M, Li W, Yao T, Wu JW, et al. Crystal structure of a UBP-family deubiquitinating enzyme in isolation and in complex with ubiquitin aldehyde. *Cell* 2002;111:1041–54.
- [23] Hu M, Li P, Song L, Jeffrey PD, Chenova TA, Wilkinson KD, et al. Structure and mechanisms of the proteasome-associated deubiquitinating enzyme USP14. *Embo J* 2005;24:3747–56.
- [24] Ratia K, Saikatendu KS, Santarsiero BD, Barretto N, Baker SC, Stevens RC, et al. Severe acute respiratory syndrome coronavirus papain-like protease: structure of a viral deubiquitinating enzyme. *Proc Natl Acad Sci USA* 2006;103:5717–22.
- [25] Nijman SM, Luna-Vargas MP, Velds A, Brummelkamp TR, Dirac AM, Sixma TK, et al. A genomic and functional inventory of deubiquitinating enzymes. *Cell* 2005;123:773–86.
- [26] Pui CH, Evans WE. Acute lymphoblastic leukemia. *N Engl J Med* 1998;339:605–15.
- [27] Elion GB. The purine path to chemotherapy. *Science* 1989;244:41–7.
- [28] Bromme D, Nallaseth FS, Turk B. Production and activation of recombinant papain-like cysteine proteases. *Methods* 2004;32:199–206.
- [29] Rozman J, Stojan J, Kuhelj R, Turk V, Turk B. Autocatalytic processing of recombinant human procathepsin B is a bimolecular process. *FEBS Lett* 1999;459:358–62.
- [30] Kopitar G, Dolinar M, Strukelj B, Pungercar J, Turk V. Folding and activation of human procathepsin S from inclusion bodies produced in *Escherichia coli*. *Eur J Biochem* 1996;236:558–62.
- [31] Blumberg S, Schechter I, Berger A. The purification of papain by affinity chromatography. *Eur J Biochem* 1970;15:97–102.
- [32] Turk B, Krizaj I, Kralj B, Dolenc I, Popovic T, Bieth JG, et al. Bovine stefin C, a new member of the stefin family. *J Biol Chem* 1993;268:7323–9.
- [33] Chou CY, Chang HC, Hsu WC, Lin TZ, Lin CH, Chang GG. Quaternary structure of the severe acute respiratory syndrome (SARS) coronavirus main protease. *Biochemistry* 2004;43:14958–70.
- [34] Copeland RA. *Enzymes*. New York: Wiley-VCH; 2000.
- [35] Morrison JF, Walsh CT. The behavior and significance of slow-binding enzyme inhibitors. *Adv Enzymol Relat Areas Mol Biol* 1988;61:201–301.
- [36] O'Connor KA, Roth BL. Finding new tricks for old drugs: an efficient route for public-sector drug discovery. *Nat Rev Drug Discov* 2005;4:1005–14.
- [37] Lennard L, Lilleyman JS, Van Loon J, Weinsilboum RM. Genetic variation in response to 6-mercaptopurine for childhood acute lymphoblastic leukaemia. *Lancet* 1990;336:225–9.
- [38] Yates CR, Krynetski EY, Loennechen T, Fessing MY, Tai HL, Pui CH, et al. Molecular diagnosis of thiopurine S-methyltransferase deficiency: genetic basis for azathioprine and mercaptopurine intolerance. *Ann Intern Med* 1997;126:608–14.
- [39] Evans WE, Horner M, Chu YQ, Kalwinsky D, Roberts WM. Altered mercaptopurine metabolism, toxic effects, and dosage requirement in a thiopurine methyltransferase-deficient child with acute lymphocytic leukemia. *J Pediatr* 1991;119:985–9.
- [40] Weinsilboum RM. Human pharmacogenetics: introduction. *Fed Proc* 1984;43:2295–7.
- [41] Hyslop RM, Jardine I. Metabolism of 6-thiopurines. II. Covalent binding of a 6-thiopurine metabolite to mammalian tissue protein in vivo. *J Pharmacol Exp Ther* 1981;218:629–35.
- [42] Hyslop RM, Jardine I. Metabolism of 6-thiopurines. I. Irreversible binding of a metabolite of 6-thiopurine to mammalian hepatic protein in vitro. *J Pharmacol Exp Ther* 1981;218:621–8.
- [43] Pickart CM, Rose IA. Mechanism of ubiquitin carboxyl-terminal hydrolase. Borohydride and hydroxylamine inactivate in the presence of ubiquitin. *J Biol Chem* 1986;261:10210–7.
- [44] Hershko A, Rose IA. Ubiquitin-aldehyde: a general inhibitor of ubiquitin-recycling processes. *Proc Natl Acad Sci USA* 1987;84:1829–33.
- [45] Balakirev MY, Jaquinod M, Haas AL, Chroboczek J. Deubiquitinating function of adenovirus proteinase. *J Virol* 2002;76:6323–31.
- [46] Weber JM. Adenovirus endopeptidase and its role in virus infection. *Curr Top Microbiol Immunol* 1995;199(Pt 1):227–35.
- [47] Ritchie KJ, Hahn CS, Kim KI, Yan M, Rosario D, Li L, et al. Role of ISG15 protease UBP43 (USP18) in innate immunity to viral infection. *Nat Med* 2004;10:1374–8.